Mitigation of stimulated Raman scattering in high-power fiber MOPA laser based on dual-structure fiber grating

Kerong Jiao [1,2], Qingqing Kong [1,2], Yangning Guo [1,2], Jingwei Li [1,2], Chen Wu [1,2], Zhigang Han [1,2], Rihong Zhu [1,2], and Hua Shen [1,2,*]

[1] *School of Electronic Engineering and Optoelectronic Technology, Nanjing University of Science and Technology, Nanjing 210094, China*
[2] *MIIT Key Laboratory of Advanced Solid Laser, Nanjing University of Science and Technology, Nanjing 210094, China*

*Correspondence to: Hua Shen, MIIT Key Laboratory of Advanced Solid Laser, Nanjing University of Science and Technology, Nanjing 210094, China. Email: edward_bayun@163.com

Abstract With the increasing power of fiber lasers, single chirped and titled fiber Bragg gratings (CTFBGs) cannot completely mitigate continuously enhanced system-excited stimulated Raman scattering (SRS). Although improving the loss rate of a single CTFBG or cascading multiple CTFBGs can provide better suppression of the stronger SRS, excessive insertion loss may cause significant attenuation of the output power. Confronting the challenge, we firstly present an SRS mitigation method based on dual-structured fiber grating in this paper. The dual-structure fiber grating comprises a CTFBG and a fiber Bragg

10.1017/hpl.2023.77

grating (FBG) structure, which were designed and fabricated on a passive 25/400 double-clad fiber. To evaluate the performance of the grating, a 3 kW fiber MOPA laser is established. The experimental results demonstrate that the SRS mitigation rate of the grating is greater than 30 dB (99.9%), whereas the insertion loss is only approximately 3%, thus allowing for minimal deterioration of the output power. This solves the contradiction between high suppression rate and high insertion loss faced by CTFBG, which in turn makes dual-structure fiber gratings particularly suitable for mitigating SRS in 3-5 kW high-power fiber lasers.

Key words: High-power fiber laser; Fiber optics component; Stimulated Raman scattering; Dual-structure fiber grating.

I. INTRODUCTION

Stimulated Raman scattering (SRS) is one of the main factors limiting the power enhancement of high-power fiber lasers and deteriorating the output laser beam quality [1-4]. Efficient suppression of SRS has become an urgent challenge. Owing to the advantages of small size and easy integration of fiber grating, SRS suppression technology based on fiber gratings has become a hot research topic. A method of utilizing long-period fiber gratings (LPFGs) to suppress SRS was proposed firstly [5-8]. However, since the period of the LPFG is usually on the order of sub-millimeters, the resonance of the LPFG is susceptible to drift due to environmental perturbations [9,10], which in turn leads to a decrease in the suppression of SRS. Therefore, an SRS suppression method based on chirped and tilted fiber Bragg gratings (CTFBGs) has emerged as the times require [11-13]. Compared with the LPFG, the period of the CTFBG is much smaller (on the order of hundreds of nanometers), indicating that the CTFBG is more stable. Therefore, this method has been

2

extensively developed owing to this advantage. However, as the laser power continues to enhance, the intensity of SRS becomes increasingly stronger. When the suppression ability of a single CTFBG reaches its limit, SRS cannot be completely suppressed [14-16].

Currently, two methods exist to enhance the SRS suppression rate of CTFBG. The first is the enhancement of the refractive index modulation amplitude of the CTFBG itself (by increasing the photosensitivity of the fiber or extending the exposure time of the ultraviolet (UV) laser during inscription). Although this method can increase the SRS suppression rate of the CTFBG by more than 30 dB, it also increases the laser signal loss of the CTFBG (i.e., the insertion loss of the CTFBG, which is >5%). We demonstrated this through experiments in the Part IV. The second method achieved a high SRS suppression rate by cascading several CTFBGs (multiple CTFBGs). However, this superimposes the insertion losses of individual CTFBGs, resulting in a significant increase in the insertion loss of multiple CTFBGs (>6%) [17]. Song et al. proposed a scheme of cascading multiple CTFBGs (multiplexed CTFBG) to achieve loss rate ≥25 dB and insertion loss ≤3% [18]. The loss rate and insertion loss of multiplexed CTFBG are the superposition of the loss rate and insertion loss of single CTFBGs. Therefore, this scheme does not essentially solve the contradiction between the high suppression rate and high insertion loss faced by CTFBG. To further increase the loss rate of the multiplexed CTFBG (e.g. ≥40dB), it is necessary to increase the loss rate of single CTFBGs or cascade more CTFBGs, which still leads to the increase of insertion loss of the multiplexed CTFBG. Therefore, a method is urgently required to improve the SRS suppression rate of the CTFBG without increasing the insertion loss.

Confronting this challenge, this paper, to the best of our knowledge, first presents a dual-structure fiber grating to improve the SRS suppression rate. The grating contains a CTFBG structure as well as a fiber Bragg grating (FBG) structure, where the FBG structure is immediately

3

behind the CTFBG structure. Therefore, when the signal laser passes through the dual-structure fiber grating, most of the SRS light will be filtered out after passing through the CTFBG. Furthermore, the residual SRS light will be reflected by the FBG to the CTFBG and then filtered out again by the CTFBG. This implies that the SRS light passes through the CTFBG twice while the signal laser passes only once. This is the key factor as it causes the dual-structure fiber grating to have a low insertion loss while achieving a high SRS suppression rate. A detailed design philosophy and method for the fiber grating are also proposed. Furthermore, a dual-structure fiber grating is designed and fabricated on a passive 25/400 double-clad fiber. To verify the feasibility of the proposed method, a 3 kW fiber MOPA laser is established to evaluate the performance of the fabricated fiber grating. The experimental results demonstrate that the SRS suppression rate of the dual-structure fiber grating is greater than 30 dB, while the insertion loss is approximately 3%, which is equal to that of a single CTFBG.

II. Design and Simulations

The structure of the dual-structure fiber grating and the principle of mitigating the SRS are shown in Fig.1. This type of grating consists of a CTFBG and an FBG structure. The spectra of the CTFBG and FBG are designed to cover the SRS completely. When the signal laser containing Stokes light transmits to the grating, the SRS will first be coupled by the CTFBG structure from the forward-transmitting core mode to the backward-transmitting cladding mode. In this case, the backward-transmitting cladding mode will contain most of the SRS power. Meanwhile, there is a small amount of signal laser in the backward-transmitting cladding mode due to the insertion loss of the CTFBG at the signal laser wavelength. Subsequently, when the signal laser continues to transmit to the FBG structure, the residual SRS light will be coupled to the backward-transmitting

4

core mode, which is then coupled to the cladding mode again by the CTFBG. At this time, the CTFBG couples the SRS light to the forward-transmitting cladding mode. Since the FBG hardly reflects the signal laser, only the residual SRS is present in the forward-transmitting cladding mode. Finally, cladding power strippers (CPS1 and CPS2) are used to strip the cladding mode from the fiber to suppress SRS. This implies that the Stokes light passes through the CTFBG twice, while the signal laser passes only once. Therefore, the dual-structure fiber grating exhibits a low insertion loss while achieving a high SRS mitigation rate.
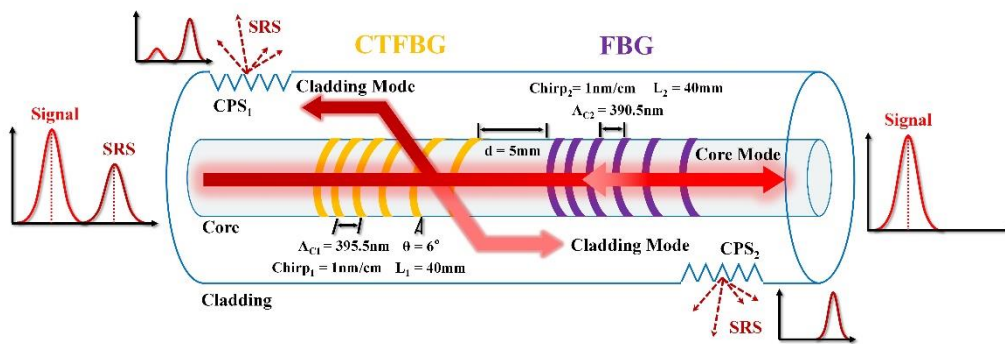

Figure 1, Schematic of the dual-structure fiber grating's structure and the principle of mitigating SRS.

To analyze the transmission and reflection spectra of dual-structure fiber grating, we need to calculate the transmission and reflection spectra of CTFBG and FBG. We first analyze the derivation of the transmission spectrum I_{T-C} and reflection spectrum I_{R-C} of CTFBG. Since the CTFBG can couple the forward-transmitting core mode to the backward-transmitting core and cladding modes. Therefore, the mode coupling equations of CTFBG can be expressed as [19,20],

$$\frac{dA^{core}}{dz} = j\sigma(z,\lambda(z),\theta)A^{core} + j\frac{s}{2}\sigma(z,\lambda(z),\theta)B^{core}e^{-2j\delta^{co-co}z} + j\sum_{i}\kappa(z,\lambda(z),\theta)B_i^{clad}e^{-2j\delta^{cl-co}z} \qquad (1.1)$$

5

$$\frac{dB^{core}}{dz} = -j\sigma(z,\lambda(z),\theta)B^{core} - j\frac{s}{2}\sigma(z,\lambda(z),\theta)A^{core}e^{2j\delta^{co-co}z} \tag{1.2}$$

$$\frac{dB_i^{clad}}{dz} = -i\sum_i\left[\kappa_i(z,\lambda(z),\theta)A^{core}e^{2j\delta^{cl-co}z}\right]. \tag{1.3}$$

A^{core}, B^{core}, and B_i^{clad} respectively represent the complex amplitudes of the forward transmission core mode, backward transmission core mode, and ith backward transmission cladding mode. λ is the wavelength, θ is the tilted angle, s represents the fringe visibility. $\sigma(z,\lambda(z),\theta)$ is the self-coupling coefficient and $\kappa_i(z,\lambda(z),\theta)$ is the cross-coupling coefficients, which can be expressed as

$$\sigma(z,\lambda(z),\theta) = \frac{\pi n_{core,eff}}{\lambda(z)}\overline{\Delta n_{core}(z)}\cos\theta\iint\limits_{core}\mathbf{e}(x,y)\mathbf{e}^*(x,y)dxdy \tag{2}$$

$$\kappa_i(z,\lambda(z),\theta) = \frac{\pi n_{core,eff}}{2\lambda(z)}\overline{\Delta n_{core}(z)}\cos\theta\iint\limits_{core}e^{i\frac{2\pi}{\Lambda_{CTFBG}(z)}x\tan\theta}\mathbf{e}(x,y)\mathbf{e}^*(x,y)dxdy, \tag{3}$$

where $n_{core,eff}$ is the effective refractive index of the fiber core, $\overline{\Delta n_{core}(z)}$ is the slow variable envelope function. $\mathbf{e}(x,y)$ is the transverse component of the fundamental mode electric field, and $\mathbf{e}^*(x,y)$ is its conjugation. $\Lambda_{CTFBG}(z)$ represents the period of CTFBG, which can be expressed as

$$\Lambda_{CTFBG}(z) = \Lambda_{C1} + \frac{Chirp_1}{2n_{core,eff}}z/\cos\theta \qquad (-\frac{L_1}{2}\leq z\leq\frac{L_1}{2}), \tag{4}$$

where Λ_{C1} is the center period of the CTFBG, $Chirp_1$ is the chirp rate of the CTFBG, and L_1 is the length of CTFBG. Further, δ^{co-co} represents the detuning coefficient between the fiber core modes

6

and δ^{cl-co} represents the detuning coefficient between the cladding modes and core modes, which can be expressed as,

$$\delta^{co-co} = \frac{2\pi}{\lambda} n_{core,eff} - \frac{\pi}{\Lambda_{CTFBG}} \tag{5}$$

$$\delta^{cl-co} = \frac{\pi}{\lambda} n_{core,eff} + \frac{\pi}{\lambda} n_{clad,eff}^{i} - \frac{\pi}{\Lambda_{CTFBG}}, \tag{6}$$

where $n_{clad,eff}^{i}$ is the effective index of the ith cladding mode. When Equations (5) and (6) are equal to 0, we can the calculate the Bragg resonance wavelength $\lambda_{B-CTFBG}$ and cladding-modes resonance wavelengths of CTFBG, which can be expressed as

$$\lambda_{B-CTFBG}(z) = 2n_{core,eff}\left(\Lambda_{C1} + \frac{Chirp_1}{2n_{core,eff}}z\right)/\cos\theta \qquad (-\frac{L_1}{2} \le z \le \frac{L_1}{2}) \tag{7}$$

$$\lambda_{clad,i}(z) = (n_{clad,eff}^{i} + n_{core,eff})\left(\Lambda_{C1} + \frac{Chirp_1}{2n_{core,eff}}z\right)/\cos\theta \qquad (-\frac{L_1}{2} \le z \le \frac{L_1}{2}). \tag{8}$$

Thus, I_{T-C} and I_{R-C} can be obtained by solving Equations (1.1)-(1.3), which can be expressed as

$$I_{T-C}(\lambda) = \frac{\left|A_{core}(\frac{L_1}{2})\right|^2}{\left|A_{core}(-\frac{L_1}{2})\right|^2} \quad I_{R-C}(\lambda) = \frac{\left|B_{core}(\frac{L_1}{2})\right|^2}{\left|A_{core}(-\frac{L_1}{2})\right|^2} \tag{9}$$

Compared to CTFBG, the derivation of the transmission spectrum I_{T-F} and reflection spectrum I_{R-F} for FBG is much simpler. FBG couples the forward-transmitting fiber core modes

7

to the backward-transmitting fiber core modes, and thus the mode coupling equation can be simplified as,

$$\frac{dA^{core}}{dz} = j\sigma(z,\lambda(z),\theta)A^{core} + j\frac{s}{2}\sigma(z,\lambda(z),\theta)B^{core}e^{-2j\delta^{co-co}z} \tag{10.1}$$

$$\frac{dB^{core}}{dz} = -j\sigma(z,\lambda(z),\theta)B^{core} - j\frac{s}{2}\sigma(z,\lambda(z),\theta)A^{core}e^{2j\delta^{co-co}z}. \tag{10.2}$$

The period of FBG can be expressed as

$$\Lambda_{FBG}(z) = \Lambda_{C2} + \frac{Chirp_2}{2n_{core,eff}}z \qquad (-\frac{L_2}{2} \leq z \leq \frac{L_2}{2}), \tag{11}$$

where Λ_{C2} is the center period of the FBG, $Chirp_2$ is the chirp rate of the FBG, and L_2 is the length of CTFBG. Furthermore, the detuning coefficient δ^{co-co} can be expressed as

$$\delta^{co-co} = \frac{2\pi}{\lambda}n_{core,eff} - \frac{\pi}{\Lambda_{FBG}}. \tag{12}$$

Thus the Bragg resonance wavelength of FBG (obtained when Equation (12) equals 0) can be expressed as

$$\lambda_{B-FBG}(z) = 2n_{core,eff}\left(\Lambda_{C2} + \frac{Chirp_2}{2n_{core,eff}}z\right) \qquad (-\frac{L_2}{2} \leq z \leq \frac{L_2}{2}) \tag{13}$$

Further, I_{T-F} and I_{R-F} can also be calculated by solving Equations (10.1)-(10.2), which can be expressed as

8

$$I_{T-F}(\lambda) = \frac{\left| A_{core}(\frac{L_2}{2}) \right|^2}{\left| A_{core}(-\frac{L_2}{2}) \right|^2} \quad I_{R-F}(\lambda) = \frac{\left| B_{core}(\frac{L_2}{2}) \right|^2}{\left| A_{core}(-\frac{L_2}{2}) \right|^2}. \tag{14}$$

Therefore, the transmission spectrum I_T of the dual-structure fiber grating, which represents the mitigation characteristics of the SRS, is determined by the transmission spectrum I_{T-C} of the CTFBG and the transmission spectrum I_{T-F} of the FBG. This can be calculated using Equation 15,

$$I_T(\lambda) = I_{T-C}(\lambda) \times I_{T-F}(\lambda). \tag{15}$$

The reflection spectrum I_R of the dual-structure fiber grating is determined by the backward-transmitting core mode. According to Fig. 1, it can be observed that the backward-transmitting core mode consists of two parts. The first part consists of the backward-transmitting core mode I_{R-C} formed by the CTFBG. The second part consists of the residual backward-transmitting core mode I_{R-C-F}, which is reflected by the FBG and immediately filtered by the CTFBG ($I_{R-C-F} = (1 - I_{T-C})^2 \times I_{R-F}$). Therefore, I_R can be calculated using Equation 5

$$I_R(\lambda) = I_{R-C}(\lambda) + I_{R-C-F}(\lambda) + 2\sqrt{I_{R-C}(\lambda)I_{R-C-F}(\lambda)} \cos\left(\frac{2\pi}{\lambda}\Delta\right), \tag{16}$$

where $\Delta = (L_1 + L_2)/2 + d$ (d is the distance between the two structures, as shown in Fig. 1). In the design of a dual-structure fiber grating, we must adhere to the principle that the intensity of the backward-transmitting core mode should be low to prevent excessive Stokes light from being reflected into the laser system (this may amplify the SRS).

9

The intensity of the backward transmitting core mode depends on the reflection spectrum of the dual-structure fiber grating. Thus, according to Equation (16), there are two main components that determine I_R, which are I_{R-C} and I_{R-C-F}. The stronger the I_{R-C} and I_{R-C-F}, the stronger the I_R. Further leads to stronger backward transmission cladding mode.

The intensity of I_{R-C} is determined by the loss rate of the CTFBG (which in turn is determined by the refractive index modulation amplitude) [13].The larger the loss rate of the CTFBG, the stronger the intensity of I_{R-C}. However, the intensity of I_{R-C} is usually below 20 dB [13,14,17], thus has a negligible effect on I_R. Furthermore, I_{R-C-F} mainly depends on two aspects. Firstly, it depends on the loss rate of the CTFBG. According to the expression of I_{R-C-F}, as the loss rate of CTFBG decreases, the I_{R-C-F} is enhanced. And subsequently causes an enhancement of the intensity of the backward transmitting core mode. In addition, the intensity of I_{R-C-F} also depends on the alignment of the spectra of CTFBG and FBG. If a mismatch between the CTFBG and FBG spectra occurs, the CTFBG will not be able to fully couple the FBG reflected backward transmitting core mode into the cladding modes. Further, there will be a part of the residual backward transmitting core mode that continues to be transmitted backward after passing through the CTFBG, which results in the backlight enhancement.

There are two main types of mismatches. Firstly, the full-width-at-half maximum (FWHM) of FBG mismatches with that of CTFBG. When the FWHM of FBG is larger than that of CTFBG, CTFBG cannot fully couple the backward transmitting core mode, reflected by FBG, to the cladding. Further results in the enhancement of the backward light. Secondly, the center wavelength of FBG mismatches with that of CTFBG. This also makes CTFBG cannot fully couple the backward transmitting to the cladding. Therefore, we need to explore the effect of the loss rate

10

of the CTFBG, full-width-at-half-maximum (FWHM) of the FBG, and center wavelength of the FBG on the dual-structure fiber grating's spectra.

The effect of the loss rate of the CTFBG on the spectra of the dual-structure fiber grating is explored first. The simulation results are shown in Fig. 2. We set the tilt angle θ of the CTFBG to 6°, period Λ_{C1} (center position) to 395.5 nm, length L_1 to 40 mm, and chirp rate to 1 nm/cm. To obtain the transmission and reflection spectra of the CTFBGs with different loss rates, we set the refractive index modulation amplitude n_1 of the CTFBGs to 0.002, 0.005, 0.007, and 0.010, respectively, as shown in Figs. 2(a) and 2(b). The center wavelength of the cladding mode resonance of the CTFBG is 1135 nm and the FWHM is approximately 13 nm, which can span the SRS spectrum. Regarding the FBG, the period Λ_{C2} is set to 390.5 nm, length L_2 to 40 mm, index modulation amplitude to 0.0007, and chirp rate to 1 nm/cm. The designed spectra are presented in Figs. 2(c) and 2(d). The calculation results show that the center wavelength of the FBG matches that of the CTFBG, and its FWHM (11.0 nm) is slightly smaller than that of the CTFBG. In addition, the reflectivity of the FBG is set to more than 20 dB to ensure a high SRS mitigation ratio for the dual-structure fiber grating. Furthermore, to reduce the length of the dual-structure fiber grating, we placed an FBG 5 mm after the CTFBG, as shown in Fig. 1. According to Equations 1 and 2, the spectra of the dual-structure fiber grating are calculated, as shown in Figs. 2(e) and 2(f). The simulation results show that the loss rate of the CTFBG significantly influences the reflection spectrum of the grating. As the loss rate decreases, the reflection spectrum intensity of the dual-structure fiber grating gradually increases, which enhances the Stokes light energy transmitted in the reverse direction in the fiber laser system, causing an SRS surge. Therefore, we hope that the loss rate of the CTFBG will be as high as possible. However, in practice, it is difficult to achieve a high loss rate by imputing the photosensitivity of the fiber and energy of the inscribing UV laser.

11

In addition, the high loss rate increases the insertion loss of the CTFBG. Thus, we control the loss rate of the CTFBG at 20dB. In this case, the reflection intensity of the dual-structure fiber grating is lower than -20 dB and the loss rate of the grating reaches 40 dB.
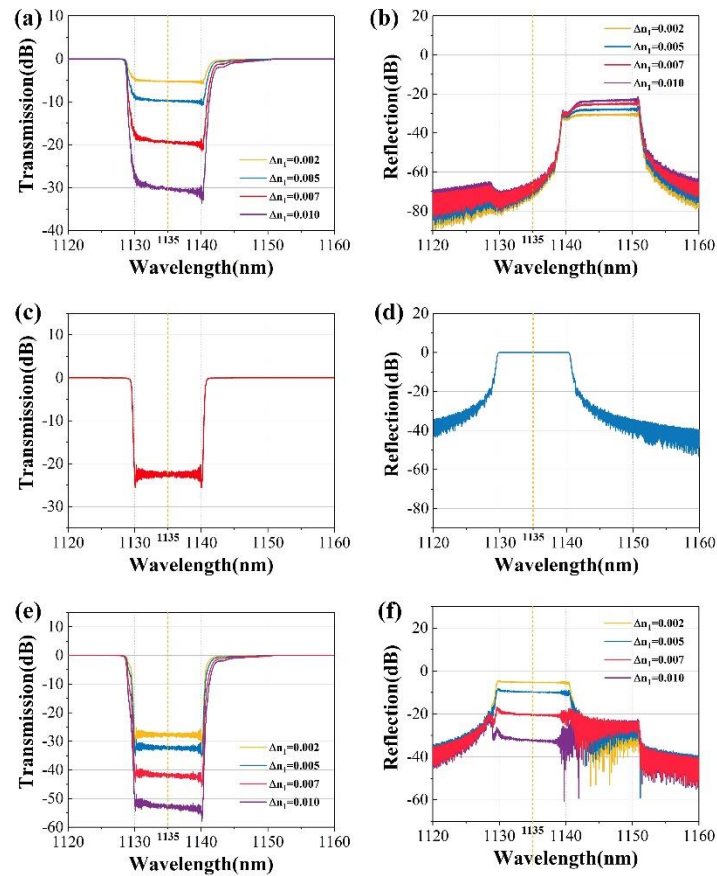

Figure 2, Influence of the CTFBG's loss rate on the dual-structure fiber grating. (a) Transmission and (b) reflection spectra of CTFBG with different refractive index modulation amplitudes. The tilt angle of CTFBG is 6°, the period is 395.5 nm, the chirp rate is 1 nm/cm, and the length is 40 mm. (c) Transmission and (d) reflection spectra of FBG. The period of FBG is 390.5nm, the chirp rate is 1nm/cm, the length is 40mm, and the refractive index modulation amplitude is 0.0007. The calculated (e) transmission and (f) reflection spectra of the dual-structure fiber grating.

12

Subsequently, the influence of FWHM of the FBG on the dual-structure fiber grating is investigated. The results are shown in Fig. 3. The refractive index modulation amplitude of the CTFBG is 0.007 (corresponding to a loss rate of 20 dB) and the other parameters are the same as before. The corresponding spectra are shown in Figs. 3(a) and 3(b). The FWHM of the FBG is varied by controlling its length, which is set to 20, 30, 40, and 50 mm, corresponded to the FWHM values of 6, 9, 11, and 14 nm, respectively. The other parameters remain unchanged, and the transmission and reflection spectra are shown in Figs. 3(c) and 3(d). The the calculated spectra of the dual-structure fiber grating are shown in Figs. 3(e) and 3(f). The simulation results show that when the FWHM of FBG is smaller than that of the CTFBG, it primarily affects the bandwidth of the dual-structure fiber grating at the highest loss rate. As the FWHM of the FBG decreases, the bandwidth at the highest loss rate of the dual-structure grating also decreases. When the FWHM of the FBG is larger than that of the CTFBG, spikes occur in the reflection spectrum of the dual-structure fiber grating. However, this violates the design principles. Therefore, the FBG length is set to 40 mm (corresponding to a bandwidth of 11.0 nm). At this point, the bandwidth at the highest loss rate of the dual-structure fiber grating could cover the SRS, and the intensity of the reflection spectrum could be controlled to values below -20 dB.
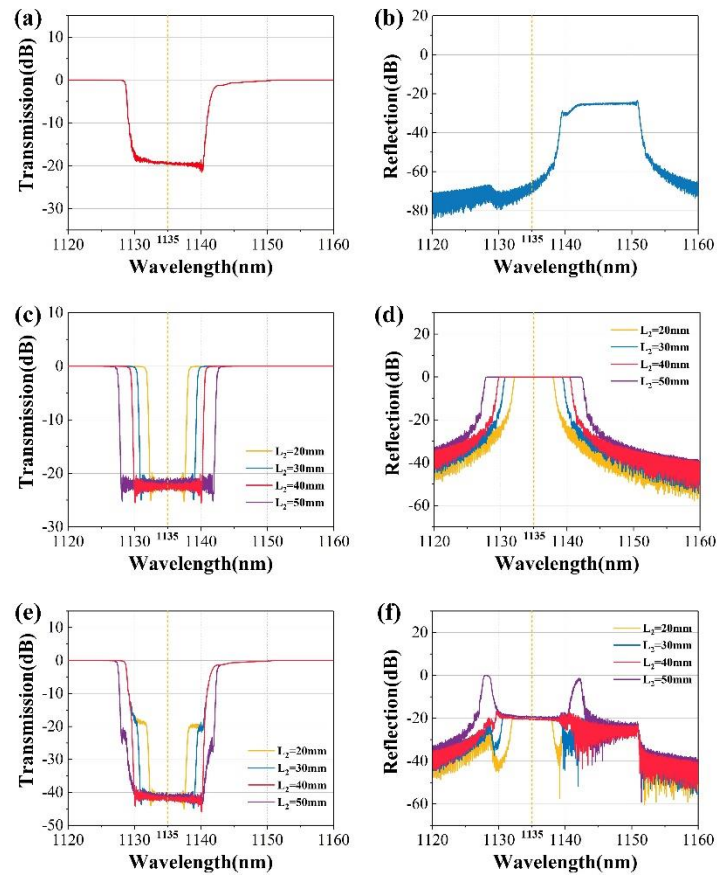
Figure 3, Influence of FBG's FWHM on dual-structure fiber grating. (a) Transmission and (b) reflection spectra of CTFBG with the refractive index modulation amplitude of 0.007 (the other parameters are the same as those in Fig. 2). (c) Transmission and (d) reflection spectra of FBG at different lengths. The period of FBG is 390.5 nm, the chirp rate is 1 nm/cm, and the refractive index modulation amplitude is 0.0007. Calculated (e) transmission and (f) reflection spectra of the dual-structure fiber grating.

Finally, we change the center wavelength of FBG by controlling its period to investigate the effect of the match between the center wavelengths of the CTFBG and FBG on the dual-structure fiber grating. The parameters of the CTFBG are the same as before, and the spectral data are shown in Figs. 4(a) and 4(b). The period of FBG is set to 389.9, 390.2, 390.5, and 390.9 nm, which corresponded to the center wavelengths of 1133, 1134, 1135, and 1136 nm. The other FBG

14

parameters are the same as before, and the simulation spectra are shown in Figs. 4(c) and 4(b). Therefore, we can calculate the transmission and reflection spectra of the dual-structure fiber grating as shown in Figs. 4(e) and 4(f). Large spikes appear in the reflection spectra when the center wavelength of the FBG mismatches that of the CTFBG. Unfortunately, this violates the design principles.
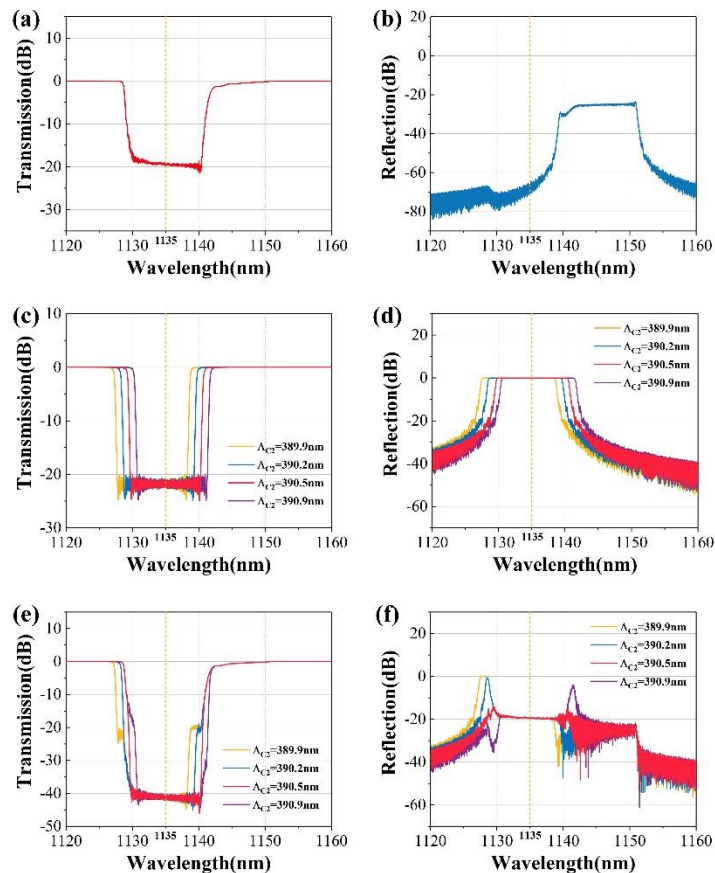

Figure 4, Influence of FBG's center wavelength on dual-structure fiber grating. (a) Transmission and (b) reflection spectra of CTFBG (the parameters are the same as those in Fig. 3). (c) Transmission and (d) reflection spectra of FBG at different periods. The length of FBG is 40 nm, the chirp rate is 1 nm/cm and the refractive index modulation amplitude is 0.0007. Calculated (e) transmission and (f) reflection spectrum of the dual-structure fiber grating.

15

In conclusion, we summarize the design concepts of dual-structure fiber gratings. First, the loss rate of CTFBG is maintained at approximately 20 dB. Second, the FWHM of the FBG should cover the SRS range as much as possible but can be slightly smaller than that of the CTFBG. Finally, the center wavelength of FBG must match that of CTFBG. Therefore, we choose the following design parameters of the CTFBG in the dual-structure fiber grating: tilt angle 6°, period 395.5 nm, chirp rate 1 nm/cm, length 40 mm, and loss rate 20 dB. Further, the design parameters of FBG are period 390.5 nm, chirp rate 1 nm/cm, length 40 mm, reflectivity >20 dB, and distance from CTFBG is 5 mm. The simulated spectra of the dual-structure fiber grating are shown in Figs. 5(a) and 5(b). The center wavelength of the fiber grating is 1135 nm, the FWHM is approximately 13.1 nm, and the loss rate is >40 dB.
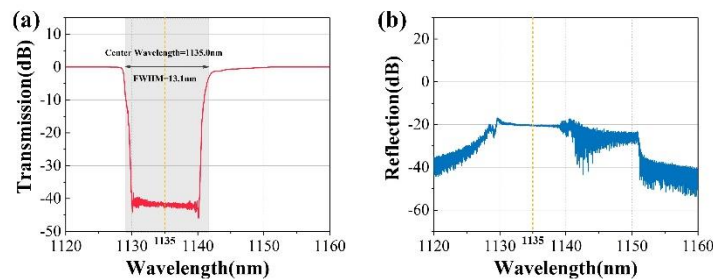

Figure 5, Design results of the dual-structure fiber grating's (a) transmission and (b) reflection spectra. The center wavelength of the designed fiber grating is 1135 nm, the FWHM is approximately 13.1 nm and the loss rate is >40 dB.

III. Fabrication

A phase mask based scanning method [13] is used to inscribe the dual-structure fiber grating and an argon-ion laser (Innova 90C FreD Ion Laser, Coherent Inc.) is utilized as the lithography laser source. According to the design parameters obtained in Part II, phase mask 1 for the CTFBG has a period Λ_{P1} of 791 nm, chirp rate $Chirp_{P1}$ of 2 nm/cm, and length L_1 of 40 mm, whereas phase

16

mask 2 for the FBG has a period Λ_{P2} of 781 nm, a chirp rate $Chirp_{P2}$ of 2 nm/cm, and a length

L_2 of 40 mm. The inscription process is divided into four steps, as shown in Fig. 6. First, the

hydrogenated fiber (18 days at 13 MPa and 40 °C, Nufern LMA-GDF-25/400-HP-M) is aligned

with Phase mask 1. Subsequently, the Phase mask 1 is rotated so that there is an angle θ_R between

it and the fiber axial direction. As the fiber is equivalent to a cylindrical lens, the interference field

incident on the fiber core will be distorted [13], thus resulting in an error between the tilt angle θ

of the CTFBG and the rotation angle θ_R. The relationship between these parameters can be

expressed using by Equation 17,

$$\theta = \frac{\pi}{2} - \arctan\left(n_{UV}\tan\theta_R\right)^{-1}, \tag{17}$$

where n_{UV} is the refractive index of the fiber core at 244 nm. Thus, to realize the inscription of the

CTFBG with tilt angle of 6°, the template is rotated to approximately 4.2° relative to the fiber. The

power of the UV laser is set to 100 mW, and the inscription speed is set to 0.0015 mm/s. This is

due to the refractive index modulation amplitude of CTFBG is large (0.007, which means that

CTFBG is difficult to inscribe), a high inscription power with low scanning speed is required to

inscribe CTFBG with high loss rate. When the UV laser power is set to 100mW (the highest

power), it is found by testing different scanning speeds that the loss rate of the inscribed CTFBG

could reach ≥20 dB only when the scanning speed is ≤0.0015 mm/s. Second, after inscribing the

CTFBG, the template is rotated parallel to the fiber. Third, the height of the template is increased

so that Phase mask 2 can be aligned with the fiber. Finally, the fiber is translated 5 mm to the left,

and the FBG inscription is initiated. The inscription speed is set to 0.006 mm/s, because the

refractive index modulation amplitude for FBG is small (0.0007, which means FBG is relatively

17

easy to inscribe), so the scanning speed could increase while the power remains unchanged. When the scanning speed is ≤0.006 mm/s, the reflectivity of the inscribed FBG can reach more than ≥20 dB. However, these parameters are not unique, if the UV power is reduced, then the scanning speed needs to be further reduced. If the UV laser with higher output power is applied, the scanning speed can be appropriately increased.
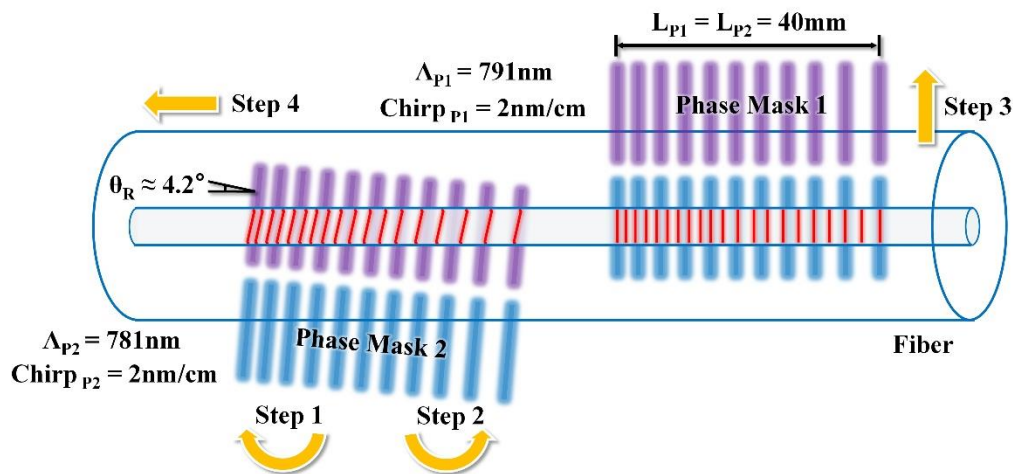

Figure 6, Schematic of the inscription process of the dual-structure fiber grating.

Furthermore, to improve the power durability of the dual-structure fiber grating, our proposed dual-annealing process, which combines constant-low-temperature and dynamic-high-temperature [13, 21, 22], is adopted. The grating is first subjected to a temperature of 60 °C for 30 days to remove residual dissociative hydrogen molecules. Then the grating is slowly heated to 350 °C at intervals of 50 °C from 23 °C, and maintained at 350 °C for 20 min before being gradually cooled to 23 °C to decrease the concentration of hydroxyl compounds. The thermal slope of the grating before annealing is approximately 0.5 °C/W, yet it is reduced to 0.016 °C/W after the heat process which allows our grating to handle a multi-kW power laser. In addition, optimizing the annealing process or utilizing femtosecond laser inscribing technology will make

18

the dual-structure fiber grating handle higher laser power. Figures 7(a) and 7(b) show the transmission and reflection spectra of the fabricated dual-structure fiber grating, respectively. The center wavelength is 1134.91 nm, the FWHM is approximately 13.9 nm. However, due to the low power of the ASE source for the measurement, the transmission spectral curve of the fabricated grating could not be fully measured, resulting in an observable loss rate ≥35 dB (99.97%). Moreover, it can be observed that no peaks appear in the reflection spectrum, which means that the dual-structure fiber grating hardly reflects the SRS light back into the laser system.
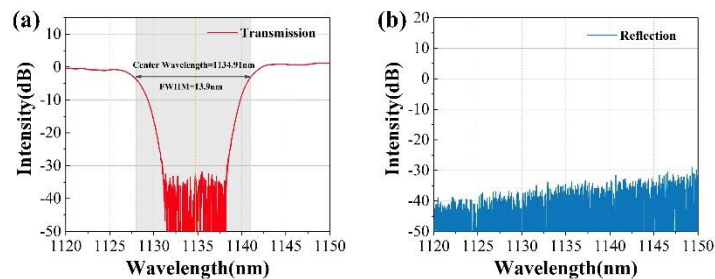

Figure 7, (a) Transmission and (b) reflection spectra of the fabricated dual-structure fiber grating. The center wavelength of the grating is 1134.91 nm, the FWHM is approximately 13.9 nm and the loss rate is more than ≥35 dB (99.97%).

IV. Experiments and results

A high-power fiber MOPA laser is established to evaluate the performance of the dual-structure fiber grating in mitigating SRS, as shown in Fig. 8. The seed consists of two 976 nm laser diodes (LDs) with an output power of 200W, a 2 × 1 combiner, a resonant cavity, and a cladding power stripper (CPS-1, for stripping the residual pump light, meanwhile, preventing the seed from being damaged by the reverse pump light generated by the amplifier). The resonant cavity is composed of a 7 m ytterbium-doped active fiber (LMA-YDF-20/400-M, Nufern Corporation) and a pair of 1080 nm FBGs. The reflectivity of the high-reflection (HR) FBG is 99.6% and that of the output-coupling (OC) FBG is 11%. The FWHMs of the HR-FBG and OC-FBG are approximately 3 nm

19

and 1 nm, respectively. And the reason we chose a 7 m ytterbium-doped fiber is mainly to shorten the fiber length of the oscillator fiber, thus increasing the SRS excitation threshold and avoiding the generated SRS light be amplified by the amplifier[23]. The final output power of the seed is 250 W. Further, the amplifier adopts a bi-directional pumping structure. The forward pumping module consists of a (6+1) ×1 combiner and four 976 nm LDs with an output power of 400 W. The reverse pumping module consists of a (8+1) ×1 combiner and eight 976 nm LDs with an output power of 400 W. The ratio of the forward and reverse pump power is 1:2 in order to suppress the transverse mode instability (TMI)[24-26]. A 15 m ytterbium-doped active fiber (LMA-YDF-25/400-M, Nufern Corporation) is utilized as the gain fiber. The amplified signal laser the outputs through the CPSs (CPS-2 and CPS-3) and through a quartz block of high power (QBH). The dual-structure fiber grating is spliced between CPS-2 and CPS-3. CPS-2 is used to strip the residual pump power, as well as the backward-transmitting cladding modes generated by the dual-structure fiber grating (containing a small fraction of the signal laser and most of the SRS light). Furthermore, CPS-3 is used to strip the forward-transmitting cladding modes (mainly including residual SRS light) produced by the dual-structure fiber grating. The output spectra of the evaluation system are measured by detecting the scattered light from the power meter using an optical spectrum analyzer (OSA). Therefore, the SRS mitigation ratio of the fiber grating can be evaluated by comparing the output spectra before and after the grating is inserted into the amplifier of the MOPA system.
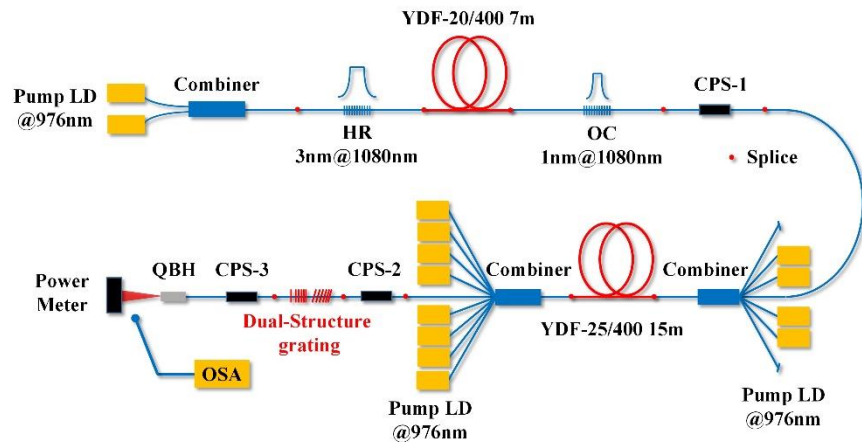
20

Figure 8, High-power fiber MOPA system for evaluating the dual-structure fiber grating's performance of mitigating SRS.

Figure 9(a) shows the output spectra of the evaluation system. When the output power exceeds 3 kW, significant SRS occurs. The center wavelength of the Stokes light is approximately 1135 nm and 55 nm away from the signal light. When the system output power reaches 3392 W (amplifier pump power of 4800W), a 22.6 dB intensity difference exists between the SRS light and signal light. Furthermore, we splice a single CTFBG between CPS-2 and CPS-3. The FWHM of the CTFBG is approximately 12.8 nm and the extinction of SRS is 18 dB (98.4%). The output spectra are shown in Fig. 9(b). It can be clearly observed that the CTFBG exhibits significant attenuation of SRS light. When the output power is lower than 3 kW, the SRS light is almost invisible. However, when the power further increase to 3256 W (amplifier pump power of 4800 W), a slight SRS appears in the spectrum. The SRS peak differs from that of the signal light by 39.1 dB. This is because the mitigation capacity of the single CTFBG reaches its limit. Furthermore, the slight decrease in the signal intensity is attributed to the insertion loss of the CTFBG. A comparison of the blue spectral curves in Figs. 9(a) and 9(b) shows that the system does not excite SRS in either state. Therefore, the insertion loss of CTFBG can be calculated as (2656 W – 2573

21

W)/2656 W $\times$ 100%=3.1%. The dual-structure fiber grating is then spliced into the system and the output spectra are shown in Fig. 9(c). The SRS light disappears when the output power reaches 3247 W (amplifier pump power of 4800 W). Moreover, the SRS mitigation ratio of dual-structure fiber grating exceeds 30 dB (99.9%). It is worth mentioning that the insertion loss of the fiber grating exhibits almost no increase compared with that of a single CTFBG, whereas the SRS mitigation ratio increases. This demonstrates the advantage of the dual-structure fiber grating. Figure 9(d) shows the output spectra of the MOPA system without fiber grating, with a single CTFBG, and a dual-structure fiber grating, respectively, when the pump power of the amplifier reaches 4800 W. The insertion loss of the dual-structure fiber grating can also be calculated by comparing the blue spectral curves in Figs. 9(a) and 9(c) as (2656 W-2570 W)/2656 W $\times$ 100% = 3.2%. In addition, TMI is the main reason to limit the further increase of the output power of the system. This is mainly due to unwanted heat generating in the fiber lase system[27-31]. First, the low efficiency of the amplifier causes part of the pump power to be converted into heat. Second, the high order modes (HOMs) excites and partially leaks at the fiber bend, which in turn causes the fiber to heat up. Third, the thermal management of the test system is not optimized, resulting in a low heat conduction rate of the fiber, which ultimately causes the heat due to heat accumulation. Aiming at this issue, we will apply tandem pumping technology and optimizing the structure of the system to increase the excitation threshold of TMI in future, thus enhance the output power and slope efficiency of the fiber laser.
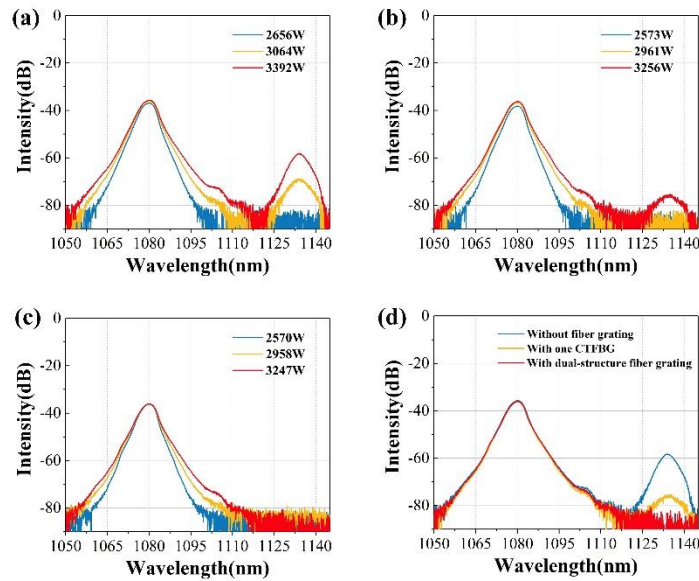
Figure 9, Output spectra of the evaluation system (a) without fiber grating, (b) with one single CTFBG, (c) with dual-structure fiber grating and (d) comparison of these three cases when the pump power of the amplifier reaches 4800W.

Figure 10 shows the slope efficiencies of the system for the three cases, which are 68.8%, 65.1%, and 65.2%, respectively. Figure 10(a) shows the evolution of the beam quality when the fiber grating is not inserted. It can be seen that the beam quality is deteriorating as the power increases. This may be caused by two reasons, the first reason is the excitation of the higher order modes (HOMs) [24], and the second reason is the excitation of the SRS effect which may slightly causes the mode distortion [32]. When the amplifier pump power reaches 4800W, the M^2 reaches 2.35. Further, the beam qualities of the MOPA system with a single CTFBG and a dual-structure fiber grating are measured and analyzed, respectively, as shown in Fig. 10(b) and 10(c). When the amplifier pump power reaches 4800W, the M^2 with a single CTFBG is 2.41 and the M^2 with a dual-structure fiber grating is 2.42. It can be clearly observed that the beam quality of the system shows a slight degradation after splicing the fiber gratings, which is caused by the distributed non-

23

rotation symmetry of the refractive index modulation of the CTFBG structure [18]. However, the beam quality of the system does not change significantly in both cases of splicing the CTFBG and dual-structure fiber grating. This is because the refractive index modulation distribution of the FBG structure is approximately rotationally symmetric. Furthermore, the refractive index modulation amplitude of FBG is also smaller than that of CTFBG, which has almost no effect on the beam quality. This is another advantage of the dual-structure fiber grating.
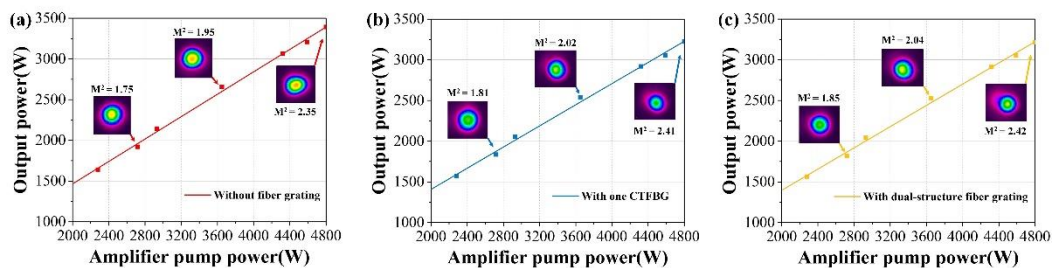

Figure 10, Output power versus amplifier pump power of the three cases. The slope efficiencies of the system for the three cases are 68.8%, 65.1%, and 65.2%, respectively. And the M2 of MOPA system for the three conditions (amplifier pump power of 4800 W) are 2.36, 2.41, and 2.42, respectively.

We further test the influence on SRS mitigation when the center wavelength of the CTFBG mismatches that of the FBG. Figures 11(a) and 11(b) show the transmission and reflection spectra of the dual-structure fiber grating when a mismatch occurs. Due to the mismatch in the center wavelength, the reflection spectrum of the fiber grating yields a peak at 1137 nm. Figure 11(c) shows the output spectra after connecting the fiber grating to the MOPA system. When the laser power is below 3 kW, the mismatched dual-structure fiber grating exhibits a good mitigation ratio. However, when the laser power is further increased to 3244 W (amplifier pump power of 4800 W), the system excites the SRS light at 1137 nm again. This is due to the mismatched fiber grating coupling of non-negligible SRS light into the backward-transmission core mode, which in turn

24

causes the backward SRS light to be amplified by the laser system. This phenomenon is similar to that observed when using CTFBGs with a small tilt angle to suppress SRS (CTFBGs with small tilt angles also couple non-negligible SRS into the backward-transmission core mode) [16, 33]. The experimental results demonstrate the necessity for the alignment of the CTFBG and FBG in the dual-structure fiber grating.
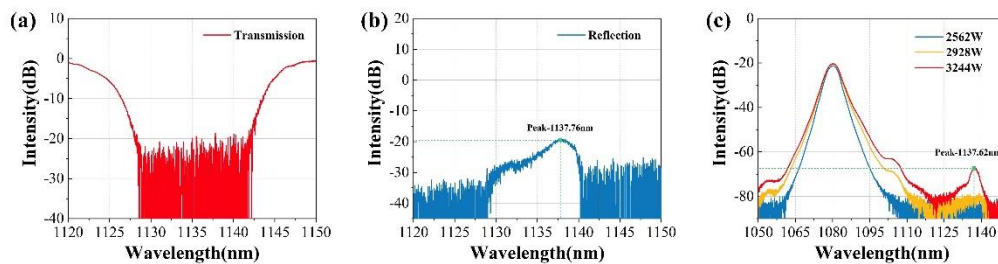

Figure 11, (a) Transmission and (b) reflection spectra of the mismatched dual-structure fiber grating. (c) Output spectra of the evaluation system with the mismatched dual-structure fiber grating.

In addition, to demonstrate that the insertion loss of CTFBG enhances with the increase of loss rate, we further fabricated three 6° CTFBGs with loss rates approximately 30 dB and measured their insertion loss. The loss rates of CTFBG-1, CTFBG-2, and CTFBG-3 are 32dB, 29.5dB, and 30dB, respectively. Furthermore, the transmission spectra of the three CTFBGs are shown in Fig. 3.According to the previous experiments, when the output power of the fiber MOPA laser system ≤2656W, there is no SRS effect in the output laser spectrum. Therefore, at this power, if the output power of the system decreases after inserting the CTFBGs, it is only caused by the insertion loss of the CTFBGs. Then the insertion loss of each of the three CTFBGs can be calculated. Table 1 shows the output powers and insertion losses of the system before and after inserting the three CTFBGs. The insertion loss of CTFBG-1 is 6.70%, that of CTFBG-2 is 6.10%, and that of CTFBG-3 is 6.33%. The experiment results indicate that the insertion loss of CTFBG is

proportional to the loss rate. Higher the loss rate brings a higher insertion loss. When the loss rate of CTFBG reaches 30dB, its insertion loss will be more than 6%. This further demonstrates that enhanced refractive index modulation amplitude leads to increased CTFBG insertion loss.
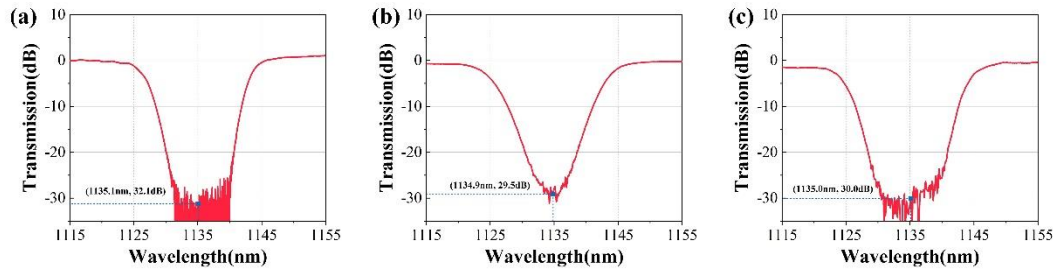

Figure 12, Transmission spectra (a) CTFBG-1, (b) CTFBG-2, and (c) CTFBG-3. The loss rates are 32dB, 29.5dB, and 30dB, respectively.

Table 1 Insertion loss with no CTFBG, with CTFBG-1, with CTFBG-2, and with CTFBG-3

	No CTFBG	CTFBG-1	CTFBG-2	CTFBG-3
Output Power (W)	2656	2478	2494	2488
Insertion Loss (%)	0	6.70	6.10	6.33

V. Conclusion

In summary, a dual-structure fiber grating consisting of CTFBG and FBG structure is proposed firstly to achieve a high SRS suppression rate. To effectively demonstrate this, the dual-structure fiber grating must satisfy the following three conditions. First, the loss rate of the CTFBG is maintained at approximately 20 dB. Second, the FWHM of the FBG should cover the SRS range as much as possible but be slightly smaller than that of the CTFBG. Finally, the center wavelength of FBG must match that of CTFBG. Based on the aforementioned design strategies, a dual-

26

structure fiber grating with an SRS suppression rate >35 dB (99.97%) is designed and fabricated on a passive 25/400 double-clad fiber. Moreover, there is no reflection peak in the reflection spectrum of the grating. Furthermore, a 3 kW fiber MOPA laser is established to evaluate the performance of the fabricated grating. Experimental results demonstrate that the SRS suppression rate of the grating is greater than 30 dB (99.9%), whereas the insertion loss is only approximately 3%, thus allowing for minimal deterioration of the output power. Moreover, we experimentally investigate the effects of CTFBG mismatches with FBG on high power fiber lasers. The proposed method solves the contradiction between the high suppression rate and high insertion loss faced by the CTFBG, which in turn makes the dual-structure fiber gratings particularly suitable for suppressing SRS in 3-5 kW high-power fiber lasers. Furthermore, the FBG can also be cascaded with the LPFG to improve the SRS suppression rate of the LPFG in future.

Acknowledgement

References

[1] W. Liu, P. Ma, H. Lv, J. Xu, P. Zhou, and Z. Jiang, "General analysis of SRS-limited high-power fiber lasers and design strategy", Opt. Express 24, 26715-26721 (2016).

[2] W. Liu, P. Ma, H. Lv, J. Xu, P. Zhou, and Z. Jiang, "Investigation of stimulated Raman scattering effect in high-power fiber amplifiers seeded by narrow-band filtered superfluorescent source", Opt. Express 24, 8708-8717 (2016).

[3] Q. Chu, Q. Shu, Z. Chen, F. Li, D. Yan, C. Guo, H. Lin, J. Wang, F. Jing, C. Tang, and R. Tao, "Experimental study of mode distortion induced by stimulated Raman scattering in high-power fiber amplifiers", Photon. Res. 8, 595-600 (2020).

[4] Z. Wang, W. Yu, J. Tian, T. Qi, D. Li, Q. Xiao, P. Yan, M. Gong, "5.12 kW tandem-pumped fiber amplifier seeded by random fiber laser with high suppression of stimulated Raman scattering", IEEE J. Quantum Electron. 57, 6800109 (2021).

[5] D. Nodop, C. Jauregui, F. Jansen, J. Limpert, and A. Tünnermann, "Suppression of stimulated Raman scattering employing long period gratings in double-clad fiber amplifiers", Opt. Lett. 35, 2982-2984 (2010).

[6] K. Jiao, H. Shen, Z. Guan, F. Yang, and R. Zhu, "Suppressing stimulated Raman scattering in kW-level continuous-wave MOPA fiber laser based on long-period fiber gratings", Opt. Express 28, 6048-6063 (2020).

[7] Q. Hu, X. Zhao, X. Tian, H. Li, M. Wang, Z. Wang, and X. Xu, "Raman suppression in 5 kW fiber amplifier using long period fiber grating fabricated by CO2 laser", Opt. Laser Technol. 145, 107484 (2022).

[8] Q. Hu, X. Tian, X. Zhao, M. Wang, X. Xi, Z. Wang, and X. Xu, "Fabrication of cascaded wideband LPFGs by CO_2 laser and Raman suppression in a 5 kW one-stage MOPA fiber laser", Opt. Laser Technol. 150, 107984 (2022).

[9] Y. Zhao, S. Liu, J. Luo, Y. Chen, C. Fu, C. Xiong, Y. Wang, S. Jing, Z. Bai, C. Liao, and Y. Wang, "Torsion, refractive index, and temperature sensors based on an improved helical long period fiber grating", J. Lightwave Technol. 38, 2504-2510 (2020).

28

[10] K. Tian, Z. Zhao, M. Zhang, M. Zhang, E. Lewis, G. Farrell, and P. Wang, "A long-period fiber grating sensor based on a core-cladding misalignment structure", J. Lightwave Technol. 40, 5316-5321 (2022).

[11] M. Wang, Y. Zhang, Z. Wang, J. Sun, J. Cao, J. Leng, X. Gu, and X. Xu, "Fabrication of chirped and tilted fiber Bragg gratings and suppression of stimulated Raman scattering in fiber amplifiers", Opt. Express 25, 1529-1534 (2017).

[12] M. Wang, Z. Wang, L. Liu, Q. Hu, H. Xiao, and X. Xu, "Effective suppression of stimulated Raman scattering in half 10 kW tandem pumping fiber lasers using chirped and tilted fiber Bragg gratings", Photon. Res. 7, 167-171 (2019).

[13] K. Jiao, J. Shu, H. Shen, Z. Guan, F. Yang and R. Zhu, "Fabrication of kW-level chirped and tilted fiber Bragg gratings and filtering of stimulated Raman scattering in high-power CW oscillators", High Power Laser Sci. Eng. 7, e31 (2019).

[14] M. Wang, L. Liu, Z. F. Wang, X. Xi, and X. Xu, "Mitigation of stimulated Raman scattering in kilowatt-level diode-pumped fiber amplifiers with chirped and tilted fiber Bragg gratings", High Power Laser Sci. Eng. 7, e18 (2019).

[15] W. Lin, M. Desjardins-Carrière, B. Sévigny, J. Magné, and M. Rochette, "Raman suppression within the gain fiber of high-power fiber lasers", Appl. Opt. 59, 9660-9666 (2020).

[16] X. Tian, X. Zhao, M. Wang, Q. Hu, H. Li, B. Rao, H. Xiao, and Z. Wang, "Influence of Bragg reflection of chirped tilted fiber Bragg grating on Raman suppression in high-power tandem pumping fiber amplifiers", Opt. Express 28, 19508-19517 (2020).

[17] X. Zhao, X. Tian, M. Wang, H. Li, B. Rao, and Z. Wang, "Design and fabrication of wideband chirped tilted fiber Bragg gratings", Opt. Laser Technol. 148, 107790 (2022).

[18] H. Q. Song, D. L. Yan, W. J. Wu, B. J. Shen, X. Feng, Y. Liu, L. Li, Q. H. Chu, M. Li, J. J. Wang, and R. M. Tao, "SRS suppression in multi-kW fiber lasers with a multiplexed CTFBG", Opt. Express 29, 20535-20544 (2021).

[19] T. Erdogan, "Fiber grating spectra", J. Lightw. Technol. 15, 1277-1294 (1997).

[20] T. Erdogan, "Cladding-mode resonances in short- and long-period fiber grating filters", J. Opt. Soc. Am. A 14, 1760-1773 (1997).

[21] Y. Bian, K. Jiao, X. Wu, H. Shen, F. Yang and R. Zhu, "Utilizing phase-shifted long-period fiber grating to suppress spectral broadening of a high-power fiber MOPA laser system", High Power Laser Sci. Eng. 9, e39 (2021).

[22] K. Jiao, H. Shen, F. Yang, X. Wu, Y. Bian and R. Zhu, "Optimizing output spectral linewidth of fiber laser utilizing phase-shifted long-period fiber grating", Opt. Laser Technol. 142, 107221 (2021).

[23] Y. H. Zheng, Z. G. Han, Y. L. Li, F. X. Li, H. Y. Wang, and R. H. Zhu, "3.1 kW 1050 nm narrow linewidth pumping-sharing oscillator-amplifier with an optical signal-to-noise ratio of 45.5 dB", Opt. Express, 30(8), 12670-12683 (2022).

[24] F. X. Li, Z. G. Han, J. L. Chen, J. B. Li, H. Y. Wang, Y. H. Zheng, M. J. Yan, and R. H. Zhu, "Interaction between inter-modal four-wave mixing and stimulated Raman scattering in high-power fiber lasers", Laser Phys. Lett., 20, 085102-1-9 (2023).

[25] Q. H. Chu, R. M. Tao, C. Y. Li, H. H. Lin, Y. Y. Wang, C. Guo, J. J. Wang, F. Jing and C. X. Tang, "Experimental study of the influence of mode excitation on mode instability in high power fiber amplifier", Scientific Reports, 9, 9936-1-7 (2019).

[26] R. M. Tao, P. F. Ma, X. L. Wang, P. Zhou, and Z. J. Liu, "Theoretical study of pump power distribution on modal instabilities in high power fiber amplifiers", Laser Phys. Lett., 14, 025002-1-5 (2017).

[27] A. V. Smith, and J. J. Smith, "Mode instability in high power fiber amplifiers", Opt. Express, 19(11), 10180-10192 (2011).

[28] C. X. Yu, O. Shatrovoy, T. Y. Fan, and T. F. Taunay, "Diode-pumped narrow linewidth multi-kilowatt metalized Yb fiber amplifier", Opt. Lett. 41(22), 5202-5205 (2016).

[29] C. Jaugegui, C. Stihler, and J. Limpert, "Transverse mode instability", Advances in Optics and Photonics, 12(2), 429-484 (2020).

[30] L. Dong, "Transverse mode instability considering bend loss and heat load", Opt. Express 31(12), 20480-20488 (2023).

[31] V. Distler, F. Möller, M. Strecker, G. P. Vega, T. Walbaum, and T. Schreiber, "Transverse mode instability in a passive fiber induced by stimulated Raman scattering", Opt. Express 28(15), 22819-22828 (2020).

[32] Q. H. Chu, Q. Shu, Z. Chen, F. Li, D. L. Yan, C. Guo, H. H. Lin, J. J. Wang, F. Jing, C. X. Tang, and R. M. Tao, "Experimental study of mode distortion induced by stimulated Raman scattering in high-power fiber amplifiers", Photon. Res., 8, 595-600 (2020).

[33] F. Liu, T. Guo, C. Wu, B. Guan, C. Lu, H. Tam, and J. Albert, "Wideband-adjustable reflection-suppressed rejection filters using chirped and tilted fiber gratings", Opt. Express 22, 24430-24438 (2014).